Color conductivity and evolution of the minijet plasma

K. J. Eskola* and M. Gyulassy†
Nuclear Science Division, Lawrence Berkeley Laboratory, Berkeley, California 94720
(Received 12 January 1993)

The early evolution of the gluon plasma produced in ultrarelativistic nuclear collisions is investigated via chromoviscous hydrodynamics. The initial conditions are determined by perturbative QCD minijet production including nuclear shadowing of the parton distributions. The analog of Ohmic heating is shown to damp rapidly any chromoelectric fields in the plasma. In the context of the flux tube models for beam jet fragmentation this damping is shown to suppress pair production processes, decrease transverse energy production, and reduce the quark-gluon chemical equilibration rate. Possible implications for dilepton production are noted.

PACS number(s): 25.75.+r

I. INTRODUCTION

Perturbative QCD (pQCD) predicts that in central collisions of ultrarelativistic nuclei at the Brookhaven Relativistic Heavy Ion Collider (RHIC) and higher energies (Au+Au at $\sqrt{s} > 100A$ GeV) hundreds of "minijet" gluons with $p_T \geq p_0 \sim 2$ GeV will be produced per unit rapidity [1–8]. This minijet system forms at very early times, $1/p_0 \sim 0.1$ fm, an extremely dense gluon plasma. The initial energy density is expected to be at least an order of magnitude above the critical value $\epsilon_c \sim 2$ GeV/fm^3 associated with deconfinement transition in QCD. This expectation has motivated an extensive experimental search for this new form of matter at RHIC and the CERN Large Hadron Collider (LHC) (see recent reviews and references in [9]).

In this paper we investigate possible consequences of one of the unique characteristics of the perturbative plasma phase of QCD matter, namely, *color conductivity* [10–12]. We calculate the evolution of the minijet plasma and transverse energy production per unit rapidity, dE_T/dy, in chromoviscous hydrodynamics [10, 12–14]. Analogous to Abelian plasmas, a finite color conductivity, $\sigma_c(T)$, leads to an induced color current, $\mathbf{J}^a$, proportional to an applied chromoelectric field, $\mathbf{E}^a$, according to a generalized Ohm's law, $J^a = \sigma_c E^a$. While no direct observation of color fields are possible because of their gauge rotation dependence, the consequences of a large chromoelectric energy density, $\epsilon_f = E^a E^a/2$, may be observable indirectly through the phenomenon of Ohmic heating [13]:

$$\frac{d\epsilon_f}{d\tau} = -J^a E^a = -2\sigma_c \epsilon_f \ . \tag{1}$$

Ohmic heating can, however, only occur if (in some fixed gauge) a mean field, E^a, is applied to the plasma for a time long compared to the typical collision time. In nuclear reactions such a possibility may arise because in addition to perturbative minijet production the projectile and target nuclei can be excited into color configurations by multiple soft gluon exchange. The two receding Lorentz contracted nuclei may then form a color capacitor system with a mean chromoelectric field, $E^a = gQ^a/A_\perp$, pointing along the beam axis and confined to a transverse area of the beam nucleus, $A_\perp \approx 4A^{2/3}$ fm^2. The decay of that field through pair production of low p_T partons [15–19] is inherently a relatively slow (few fm) process compared to the minijet time scale, $1/p_0$. Therefore, the minijet partons may evolve in that "external" field for a few fm. If the color excitation is assumed to proceed as a random walk in color space, then the mean square charge, Q^aQ^a, of each nucleus scales proportional to the number of binary inelastic $N+N$ interactions in central $A+A$ reactions, i.e., $A^{4/3}$. The gauge invariant field energy density, $\epsilon_f = E^2/2$, then also scales as $A^{4/3}$ in this model.

The above flux tube model has been applied to describe beam jet fragmentation in nuclear collisions at lower (the CERN SPS) energies where minijet production can be ignored. See Refs. [13, 18, 20] for a more detailed discussion and formulation. This model is a generalization of the familiar Lund string model [21] widely used for e^+e^- and pp reactions. While other models exist, e.g., [22], to describe beam jet fragmentation which do not assume explicitly the existence of a mean chromoelectric field, in this paper we restrict our considerations to the flux tube model for beam jets since the role of Ohmic heating is most apparent in that case.

Previous studies [13] of the role of color conductivity concentrated on nuclear reactions at lower ($\sqrt{s} < 20A$ GeV) energies with initial conditions determined by the above beam jet fragmentation model. The aim of this work is to extend those studies to collider energies, where the initial conditions are determined instead by pQCD minijet production. Because of the much higher density of partons carrying chromoelectric charge, the color conductivity should be considerably larger in the mini-

*Permanent address: Laboratory of High Energy Physics, University of Helsinki, P.O. Box 9, SF-00014 Helsinki, Finland.
†Permanent address: Physics Department, Pupin Lab, Columbia University, New York, NY 10027.

jet plasma, and its effects may therefore be more pronounced.

Linear response theory in the relaxation time approximation leads to the following estimate of the color conductivity in a pure gluon plasma [10–12]:

$$\begin{aligned}\sigma_{\rm c}^g(T) &= \tau_g \omega_{\rm pl}^2 \\ &\approx [4\alpha_{\rm s}^2 \ln(1/\alpha_{\rm s})T]^{-1}(4\pi\alpha_{\rm s}T^2/3) \\ &\approx T/[\alpha_{\rm s}\ln(1/\alpha_{\rm s})] \ , \end{aligned} \tag{2}$$

where $\omega_{\rm pl}$ is the plasma frequency and τ_g is the gluon momentum relaxation time. In a perturbative plasma at very high temperatures that relaxation time in the leading log approximation has been estimated to be [23]

$$\tau_g^{-1} \approx 4T\alpha_{\rm s}^2 \ln(1/\alpha_{\rm s}). \tag{3}$$

However, uncertainties in this estimate at attainable temperatures $T \sim 300-500$ MeV due to higher order contributions and nonequilibrium effects limit this to be only an order of magnitude estimate. We have therefore varied the conductivity over a wide range in our calculations.

Because $\sigma_{\rm c}^g$ is proportional to the momentum relaxation time, τ_g, the evolution of the system must also take into account other transport coefficients of the same order. The most important one is shear viscosity [24, 25, 14, 23], $\eta_g \approx \tau_g \epsilon/3$. Again in the leading log approximation [23], the shear viscosity in a pure glue plasma is

$$\eta \approx T^3/[3\alpha_{\rm s}^2 \ln(1/\alpha_{\rm s})], \tag{4}$$

with a similar theoretical uncertainty. For a given ratio of quark to gluon energy densities ϵ_q/ϵ_g, collisions between gluons and quarks decreases the viscosity by a factor $1/[1+\frac{4}{9}(\epsilon_q/\epsilon_g)]$. In chemical equilibrium $\epsilon_q/\epsilon_g = \frac{21}{16}$. However, the minijet initial conditions correspond to a plasma far out of chemical equilibrium with $\epsilon_q/\epsilon_g \approx \frac{1}{3}$ as we show below. Therefore, the early evolution of the gluon plasma is dominated by gg processes. Numerically, all perturbative estimates indicate that η is very large, and thus viscous dissipative effects must be included in the early evolution of the plasma [14].

Unlike gluons, quarks and antiquarks are only rarely produced as minijets. They form essentially a free streaming gas because their mean free paths are significantly longer than for gluons ($\tau_q \sim \frac{9}{4}\tau_g$) because of their smaller color charge. Also, the chemical equilibration time due to $g \to q\bar{q}$ and $gg \to q\bar{q}$ is perturbatively much longer than the gluon momentum degradation time τ_g due to $gg \to gg$ processes. We therefore concentrate on the nontrivial evolution of the gluon plasma treating the quark-antiquark gas as a decoupled free streaming gas up to $\sim 1-2$ fm. As a further simplification we adopt longitudinal boost invariant (Bjorken [26]) boundary conditions, which is approximately valid over a few units of rapidity in the c.m. We neglect also transverse expansion, thereby limiting the present study to central collisions of the heaviest nuclei.

II. CHROMOVISCOUS HYDRODYNAMICS

Under the simplifying assumption discussed in the Introduction the chromoviscous-hydrodynamic equations [10, 12–14] reduce to

$$\frac{d\epsilon_g}{d\tau} + \frac{\epsilon_g + P_g}{\tau} = \frac{4}{3}\frac{\eta_g}{\tau^2} + 2\sigma_{\rm c}^g \epsilon_f + S_{\rm s}^g + S_{\rm h}^g, \tag{5}$$

$$\frac{d\epsilon_q}{d\tau} + \frac{\epsilon_q}{\tau} = 2\sigma_{\rm c}^q \epsilon_f + S_{\rm s}^q + S_{\rm h}^q, \tag{6}$$

where ϵ_g and P_g are the proper energy density and pressure in the gluon plasma, ϵ_q is the proper energy density of the free streaming quark-antiquark gas, $\sigma_{\rm c}^i$ are the color conductivities, and $S_{\rm s}^i$ and $S_{\rm h}^i$ are source terms due to soft and hard mechanisms for partons $i = g, q$. As noted above, we expect the dominant source of energy per unit volume per unit time at collider energies to be due to minijets. That source term will be constructed in the next section. Without the Ohmic heating Eq. (5) reduces to ordinary viscous hydrodynamics [14]. Chromohydrodynamics only applies if there exist a source of chromoelectric field. As noted in the Introduction in the context of dynamical flux tube models [13, 18, 20] such a source may arise naturally due to the beam jets.

In the absence of minijets, the chromoelectric field left in the wake of the receding nuclei decays via the Schwinger pair-production mechanism in the flux tube model [13, 15–18]. Dimensional analysis alone constrains the rate of converting field energy density into parton kinetic energy density to be of the form

$$S_{\rm s}(\tau) = \kappa(2\epsilon_f)^{5/4} \equiv \sigma_v E^2 \ , \tag{7}$$

where $\kappa = \kappa_g + \kappa_q$ is a constant, and $\sigma_v(\tau) = \kappa(2\epsilon_f)^{1/4}$ can be interpreted as the vacuum conductivity [13]. In an Abelian approximation where bosons have the same color charge as fermions, the field decays dominantly into $q\bar{q}$ pairs with $\kappa_q/\kappa_g \approx 1.2\ N_f$, where $N_f \approx 2.5$ is the effective number of quark flavors. However, in SU(3) gluons have larger color charge than quarks and antiquarks and gg and $q\bar{q}$ pair-production rates are comparable with $\kappa_q/\kappa_g \approx 0.4 N_f$ [17, 27]. Because the initial quark minijet density is so small and out of chemical equilibrium, even if the Abelian approximation for κ_i is used to overestimate the $q\bar{q}$ production rate, quarks turn out to play a very minor role during the early evolution and remain far out of chemical equilibrium. Combining the decay rates due to pair production and Ohmic heating, the decay of the field energy density is controlled by

$$\frac{d\epsilon_f}{d\tau} = -J_{\rm ind}^a E^a = -(\sigma_v + \sigma_{\rm c})2\epsilon_f \ , \tag{8}$$

where the full induced current

$$J_{\rm ind}^a = [\kappa(2\epsilon_f)^{1/4} + \sigma_{\rm c}]E^a \ , \tag{9}$$

is a sum of the vacuum polarization current and the induced conductive current. Note that both σ_v and $\sigma_{\rm c}$ are time dependent.

Equations (5), (6), and (8) are more general than the one studied in [13] by the inclusion of the viscous reheating term, the minijet source term, and the decoupling of the quark and gluon components. The left-hand side describes the cooling of the plasma due to the one-dimensional boost invariant expansion as well as to the

PdV work done by the gluon plasma as it expands. As emphasized in [14], the use of the Navier-Stokes corrections only makes sense as long as the correction to the pressure term is small. However, for very early times such that $P < 4\eta/3\tau$, both the pressure and viscosity terms in the gluon equation must be set to zero. This is because a long relaxation time in the kinetic gas limit can at most negate the PdV work done in ideal hydrodynamics. Physically this corresponds simply to free streaming. At such early times both the quark and gluon energy densities decrease only because of longitudinal expansion according to the boost invariant boundary conditions.

III. MINIJET SOURCE TERM

Minijets are unresolved pQCD jets with $p_T \geq p_0 \approx 2$ GeV. The scale p_0, separating hard and soft interactions, must be determined phenomenologically in conjunction with a nonperturbative model for beam jet fragmentation. In Refs. [5–7, 28] an extensive comparison with data both at low and collider energies showed that the value $p_0 = 2$ GeV together with the Lund [21] type (flux tube) hadronization model could account well for the observed $\sqrt{s}$ dependence of transverse momentum distributions, the rise in the central rapidity densities, enhanced multiplicity fluctuations, and the flavor dependence of the rise in transverse momentum as a function of multiplicity in $p\bar{p}$ reactions. Other formulations [29] of the soft hadronization dynamics [22] find consistency with the data with $p_0 \approx 1.5$ GeV.

In the first approximation all the minijets in a nuclear collision can be viewed as being produced instantly, at their formation time, $\tau = \tau_h = 1/p_0 \sim 0.1$ fm. Then, for a given scale p_0 and impact parameter $\mathbf{b}$, the initial energy density in the midrapidity frame can be estimated from the generalization of the Bjorken formula [26]

$$\epsilon_h \approx \frac{dE_T^{AA}(\mathbf{b})}{dy}\frac{1}{\pi R_A^2 \tau_h} = \frac{T_{AA}(\mathbf{b})}{\pi R_A^2 \tau_h}\sigma_{\rm jet}\langle E_T\rangle^{pp}, \quad (10)$$

where $T_{AA}(\mathbf{b})$ is the nuclear geometrical overlapping function at an impact parameter $\mathbf{b}$. For sharp sphere nuclear geometry $T_{AA}(\mathbf{b}=\mathbf{0}) \approx A^2/(\pi R_A^2)$, where $R_A \approx 1.12A^{1/3}$ (see, e.g., [3]). The inclusive minijet cross section (divided by 2) is given by

$$\sigma_{\rm jet} \equiv \sigma_{\rm jet}(\sqrt{s}, p_0) = \frac{1}{2}\int dp_T dy_1 dy_2 \frac{2\pi p_T}{\hat{s}}\Theta(p_T \geq p_0) \times \sum_{\substack{ijkl=\\ q,\bar{q},g}} x_1 f_{i/A}(x_1, p_T^2) x_2 f_{j/A}(x_2, p_T^2)\hat{\sigma}^{ij\to kl}(\hat{s},\hat{t},\hat{u}), \quad (11)$$

where $\hat{\sigma}^{ij\to kl}$ is the elementary pQCD differential cross section for the $2 \to 2$ scattering of parton i carrying a light cone fraction x_1 of the projectile and parton j carrying a light cone fraction x_2 of the target producing partons k and l with transverse momentum p_T and rapidities y_1 and y_2. The corresponding Mandelstam variables are denoted by the hatted symbols. For example, $\hat{s} = x_1 x_2 s$. Note that $T_{AA}(\mathbf{0})\sigma_{\rm jet}$ is the total number of hard collisions with $p_T \geq p_0$ in a central AA collision.

The perturbative first E_T moment per unit rapidity of the minijet cross section is given by

$$\sigma_{\rm jet}\langle E_T\rangle^{pp} = \int dp_T dy_1 dy_2 \frac{2\pi p_T}{\hat{s}} p_T \Theta(p_T \geq p_0)\Theta(p_T, y_1, y_2) \sum_{\substack{ijkl=\\ q,\bar{q},g}} x_1 f_{i/A}(x_1, p_T^2) x_2 f_{j/A}(x_2, p_T^2)\hat{\sigma}^{ij\to kl}(\hat{s},\hat{t},\hat{u}), \quad (12)$$

where $\Theta(p_T, y_1, y_2) = 1$ if $|y_1| \leq \frac{1}{2}$ and

$$-\ln\left(\frac{\sqrt{s}}{p_T} - e^{-y_1}\right) \leq y_2 \leq \ln\left(\frac{\sqrt{s}}{p_T} - e^{y_1}\right) \quad (13)$$

and vanishes otherwise. Note that $\langle E_T\rangle^{pp}$ is the average transverse energy produced as minijets per unit rapidity at $y = 0$ in one pp subcollision [3].

In Eqs. (11) and (12) it is important to take into account the nuclear modifications to the parton number densities $f_{i/A}$, especially shadowing and antishadowing. We do this by writing $f_{i/A}(x, Q^2) = R_i^A(x, Q^2) f_i(x, Q^2)$, where the ratios $R_i^A(x, Q^2)$ do depend on the scale $Q = p_T$, especially for gluons. The gluon shadowing decreases faster with increasing scale, as described in detail in [30]. However, the initial amount of gluon shadowing at 2 GeV is not known, and we use here the ansatz 1 of Ref. [30], corresponding to the assumption that the magnitude of gluon shadowing is the same as the observed shadowing of the structure function F_2 of quarks and antiquarks. The Duke-Owens set 1 [31] is used for f_i, as well as a factor $K = 2$ to account for the $O(\alpha_s^3)$ contributions to the minijet cross section.

The result of the perturbative prediction (12) is plotted in Fig. 1 as a function of nucleon-nucleon c.m. energy from RHIC to LHC energies. The influence of the assumed gluon shadowing for a gold ($A = 196$) nucleus is also shown. The contribution from gluons (via $gg \to gg$, $gq \to gq$) is clearly dominant already at RHIC energies (about 72%) and becomes even more dominant at higher energies.

Note that Eq. (10) is a good approximation for the initial energy densities only when $\tau_h \gg \delta \equiv 2R_A/\gamma$, i.e., when the finite Lorentz-contracted nuclear thickness

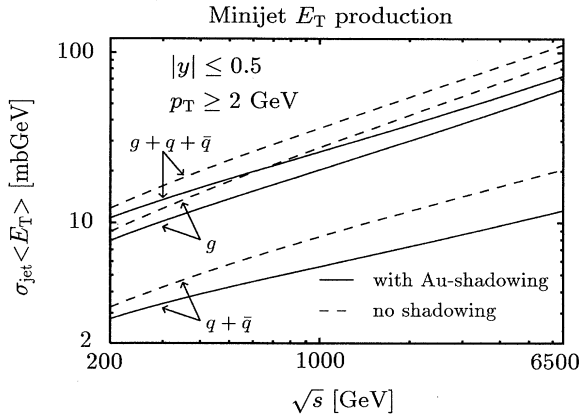

FIG. 1. The E_T weighted pQCD minijet cross section (12) in pp collisions vs cms energy is shown (dashed curves) for minijets with $p_T \geq p_0 = 2$ GeV and $|y| \leq 0.5$. Scale dependent effects of shadowing and antishadowing are taken into account nuclei by using "Ansatz 1" of Ref. [30] for gluon shadowing in $A = 196$ at $Q = p_T = 2$ GeV. The shadowed cross sections are given by the solid curves.

is small compared to the minijet formation time. For $A \sim 200$ nuclei at RHIC energies the nuclear diameter is only contracted to 0.1 fm and thus the finite transit time should be taken into account. We include the spread of production times of the minijets via

$$\tau\epsilon(\tau) = \tau_h \epsilon_h \frac{\tau - \tau_h}{\delta}. \tag{14}$$

The minijet transverse energy is thus assumed to increase linearly between τ_h and $\tau_h + \delta$. For Eqs. (5) and (6) this results in a perturbative source term of the form

$$S_h^i(\tau) = \epsilon_h^i \frac{\tau_h}{\tau} \frac{\Theta(\tau_h \leq \tau \leq \tau_h + \delta)}{\delta}, \tag{15}$$

where $i = g$ or $q + \bar{q}$. In the limit $\delta \to 0$ the perturbative source reduces to $\epsilon_h \delta(\tau - \tau_h)$.

IV. ANALYTICAL LIMITS

An instructive analytic limit of the chromohydrodynamic equations (5), (6), and (8) is obtained by setting $\delta = 0$ and neglecting the conductive and viscous terms. For this case we assume further chemical equilibrium between quarks and gluons. In this case there is only one equation for the total parton energy density $\epsilon = \epsilon_g + \epsilon_q$ in addition to the decaying field energy density one:

$$\frac{d\epsilon}{d\tau} + \frac{\epsilon + P}{\tau} = \kappa(2\epsilon_f)^{5/4} + \epsilon_h \delta(\tau - \tau_h), \tag{16}$$

$$\frac{d\epsilon_f}{d\tau} = -\kappa(2\epsilon_f)^{5/4}, \tag{17}$$

where

$$\kappa = \frac{(4\pi\alpha_s)^{5/2}\zeta(5/2)}{16\pi^3}[\gamma_F + (1 - 2^{-3/2})\gamma_B] \tag{18}$$

in the Abelian approximation of [13]. The number of helicity states of fermions (bosons) is denoted by $\gamma_{F(B)}$.

As discussed in [18], Eq. (16) can be converted into dimensionless form by writing $\epsilon_f(\tau) = \epsilon_s[f(x)]^2$ where $x = \tau/\tau_s$ and $\kappa(2\epsilon_s)^{1/4}\tau_s = 2$. Solving for ϵ_f one finds for $\tau > \tau_h$

$$\epsilon_f(\tau) = \frac{\epsilon_s}{(x - x_h + 1)^4} = \epsilon_s \left(\frac{\tau_s}{\tau - \tau_h + \tau_s}\right)^4, \tag{19}$$

where $x_h \equiv \tau_h/\tau_s$. The time τ_s is thus the typical time for the background field to decay into (anti)quarks and gluons. In the solution above, the initial energy density of the field is $\epsilon_f(\tau_h) = \epsilon_s$, i.e., we assumed the same formation time for the minijets and for the field. The

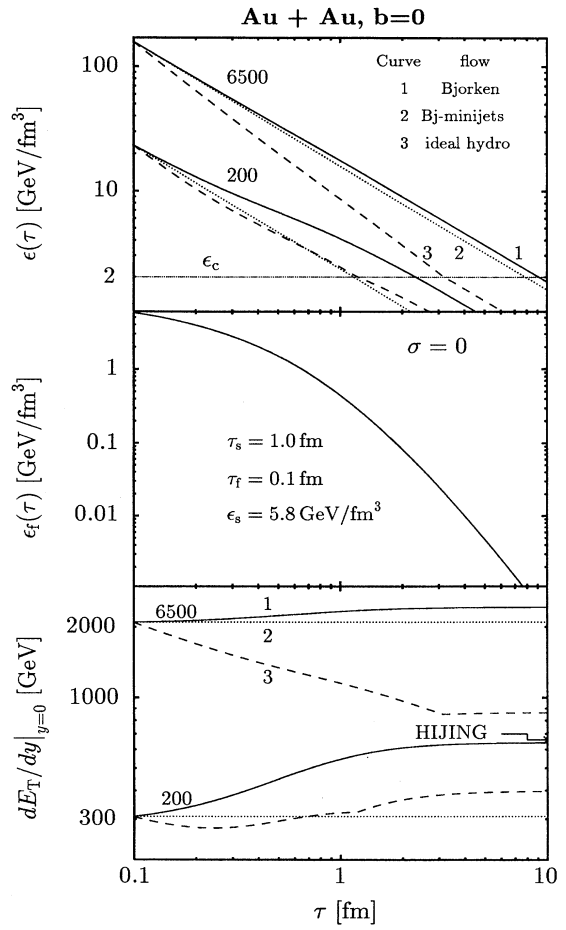

FIG. 2. Analytic solutions of the evolution equations for free streaming (Bjorken) (curves 1 and 2) and ideal hydrodynamic (curves 3) flows with minijet initial conditions are shown for central Au+Au collisions at collider energies. Top panel shows the evolution of the plasma energy density of particles, $\epsilon = \epsilon_g + \epsilon_q$, as a function of the proper time τ. Middle panel shows the evolution of the energy density of the background color field as given by Eq. (19) in the absence of conductivity with $\tau_f = 0.1$ fm, $\tau_s = 1$ fm. The bottom panel shows the evolution of the transverse energy at the midrapidity. The prediction from HIJING [5, 7] at $\sqrt{s} = 200A$ GeV is also shown.

formation time of the background field will be discussed further in the next section.

Consider next the solution in the idealized limit corresponding to free streaming. The free streaming case is referred to as "Bjorken flow." In this case there is no local pressure in the system ($P = 0$) and (16) with (19) can be integrated to yield

$$\epsilon(\tau) = \epsilon_{\rm h}\frac{\tau_{\rm h}}{\tau} + \epsilon_{\rm s}\frac{\tau_{\rm s}}{\tau}\left(x_{\rm h} + \frac{1}{3} - \frac{1 - x_{\rm h} + 4x}{3(x + 1 - x_{\rm h})^4}\right) . \quad (20)$$

This result is plotted in Fig. 2(a) as curve labeled "1." The time evolution of the particle energy density with the minijet initial conditions (10) is shown for RHIC and LHC energies. The energy density of the background field is displayed in Fig. 2(b). The final transverse energy at the central rapidity in this evolution is given by

$$\begin{aligned} E_T^0 &\equiv \left.\frac{dE_T}{dy}\right|_{y=0}^{\rm final} \\ &= \pi R_A^2 \lim_{\tau\to\infty} \epsilon(\tau)\tau \\ &= \pi R_A^2 \left\{\epsilon_{\rm h}\tau_{\rm h} + \epsilon_{\rm s}\tau_{\rm s}(x_{\rm h} + \tfrac{1}{3})\right\} . \end{aligned} \quad (21)$$

From this we can express the initial energy density of the field as

$$\epsilon_{\rm s} = \frac{E_T^0 - \langle E_T\rangle^{AA}}{\pi R_A^2(\tau_{\rm h} + \frac{1}{3}\tau_{\rm s})} = \frac{E_T^0 - \frac{A^2}{\pi R_A^2}\sigma_{\rm jet}\langle E_T\rangle^{pp}}{\pi R_A^2(\tau_{\rm h} + \frac{1}{3}\tau_{\rm s})} . \quad (22)$$

On the right-hand side there are two unknown quantities: E_T^0 and $\tau_{\rm s}$. We fix E_T^0 to agree with the Monte Carlo event generator HIJING [5, 7]. The field decay time scale $\tau_{\rm s}$ due to low p_T pair production will be taken to be 1 fm as an order of magnitude estimate.

At $\sqrt{s} = 20A$ GeV for central gold-gold collisions HIJING predicts $E_T^0 \approx 350$ GeV. At these energies minijets contribute a negligible part and we expect the flow to be a free one because of the relatively low energy densities. The minijet contribution from Eq. (12) is $\sigma_{\rm jet}\langle E_T\rangle^{pp} \approx 0.050$ GeV fm^2 at this energy. The initial energy density of the background field for $A = 196$ is then obtained as $\epsilon_{\rm s} = 5.8$ GeV/fm^3, as indicated in Fig. 2(b). The evolution of transverse energy can be expressed as

$$\left.\frac{dE_T}{dy}\right|_{y=0} = \pi R_A^2 \epsilon(\tau)\tau \quad (23)$$

and plotted as in Fig. 2(c), where we show the results again for RHIC and LHC energies. The transverse energy from HIJING at $\sqrt{s} = 200A$ GeV is also shown. Thus, we find that having fixed $\epsilon_{\rm s}$ at low energies, the model reproduces well the Monte Carlo results of HIJING at collider energies.

For comparison, in Figs. 2(a) and 2(c) we have also shown the pure minijet contribution (curves labeled 2) in the free-flowing case, i.e., $\epsilon(\tau) \sim 1/\tau$ and dE_T/dy =const. This shows that about half of the final average transverse energy of a central Au+Au collision comes from the minijets at RHIC energies, and that at LHC energies the minijets are clearly the dominant source of E_T at midrapidity. In the present model, the soft contribution is unchanged when going to higher energies and thereby, by definition, we are in agreement with the results of additive-type models like HIJING, which treat the soft contribution practically as independent of the beam energy.

Another extreme limit of interest analytically corresponds to ideal hydrodynamics when the work due to the local pressure is included. The evolution equation turns out to be solvable analytically for an ideal-gas equation of state, $P = \frac{1}{3}\epsilon$. The solution (19) of the field equation is of course unchanged. Multiplying Eq. (16) by $\tau^{4/3}$, the energy density becomes

$$\epsilon(\tau) = \epsilon_{\rm h}\left(\frac{\tau_{\rm h}}{\tau}\right)^{4/3} + \epsilon_{\rm s}\left(\frac{\tau_{\rm s}}{\tau}\right)^{4/3} 4\int_{x_{\rm h}}^{x} \frac{dy\, y^{4/3}}{(y - x_{\rm h} + 1)^5} . \quad (24)$$

The integral can be expressed in closed form

$$\begin{aligned} \epsilon(\tau) = {} & \epsilon_{\rm h}\left(\frac{\tau_{\rm h}}{\tau}\right)^{4/3} \\ & + \epsilon_{\rm s}\left(\frac{\tau_{\rm s}}{\tau}\right)^{4/3} 4[\mathcal{I}(x^{1/3}, 1 - x_{\rm h}) - \mathcal{I}(x_{\rm h}^{1/3}, 1 - x_{\rm h})], \end{aligned} \quad (25)$$

with

$$\begin{aligned} \mathcal{I}(x, a) = {} & \frac{a}{4}\frac{x}{(x^3 + a)^4} - \frac{13}{36}\frac{x}{(x^3 + a)^3} + \frac{1}{54a}\frac{x}{(x^3 + a)^2} + \frac{5}{162a^2}\frac{x}{(x^3 + a)} + \frac{5}{486a^{8/3}}\ln\frac{(x + a^{1/3})^2}{x^2 - a^{1/3}x + a^{2/3}} \\ & + \frac{5\sqrt{3}}{243a^{8/3}}\arctan\left(\frac{2x - a^{1/3}}{a^{1/3}\sqrt{3}}\right) . \end{aligned} \quad (26)$$

In the limit $\tau_{\rm h} \to 0$ and $\epsilon_{\rm h} \to 0$, we recover the results given for $\epsilon(\tau)$ in [13, 18].

The evolution of the plasma energy density in the ideal hydrodynamic limit is plotted in Fig. 2(a) (curves labeled 3). By comparing to curve 2 we see that at RHIC energies the soft source term from the decaying color field alters significantly the ideal ($\epsilon \sim 1/\tau^{4/3}$) behavior characteristic [14, 18] of hydrodynamic flow. On the other hand, at LHC energies the evolution is much closer to that ideal form because of the dominance of minijets.

In the ideal hydrodynamic expansion, work PdV is done against the pressure. As a result the transverse energy at the central rapidity unit is decreasing with time asymptotically as $dE_T/dy \sim 1/\tau^{1/3}$. This can be seen in

Fig. 2(c), where the transverse energy from Eqs. (23) and (25) is shown versus time τ. When the system becomes sufficiently dilute it has to decouple. In our calculation, we decouple the system at $\epsilon = \epsilon_c = 2$ GeV/fm^3. After this, we let the system evolve according to the equations for the free flow. This causes the kinks in the particle energy density and in the transverse energy in this model. We make no attempt to follow the evolution of the plasma through the mixed phase.

We determine the decoupling time τ_c by solving $\epsilon_c = \epsilon(\tau_c)$. Then the evolution of $\epsilon(\tau)$ is obtained from (20) by replacing ϵ_h by ϵ_c, τ_h by τ_c, and in the last term the $1-x_h$ by $[\epsilon_s/\epsilon_f(\tau_c)]^{1/4}-\tau_c/\tau_s$. The resulting evolution at $\tau \geq \tau_c$ is also shown in Figs. 2. Note that because of the much higher initial energy densities, the plasma remains coupled at LHC energies about three times longer than at RHIC.

V. COLOR CONDUCTIVITY IN A MINIJET PLASMA

We turn finally to the effect of minijet enhanced color conductivity. In the time history of a nuclear collision, the hard processes occur first and the formation of the background color field stretches over a longer period of time. We take this into account by spreading the soft source over a finite field formation time, $\tau_f \sim 1$ fm, via

$$S_s^f(\tau) = \epsilon_s \frac{1}{\tau_f}\Theta(\tau_h \leq \tau \leq \tau_f). \tag{27}$$

We assume further that the field formation time τ_f does not depend on the cms energy since it involves only wee parton dynamics.

As shown in Fig. 1, at collider energies the gluon contribution to the initial energy density is at least three times the one from quarks and antiquarks. Therefore, the system is initially far from a chemical equilibrium. Furthermore, as noted before, the mean free paths of quarks and antiquarks are perturbatively much longer than those of gluons, $\tau_q \sim 9\tau_g/4$ and gluon branching $g \to q\bar{q}$ occurs much less frequently than $g \to gg$ and $q \to qg$. Therefore we drop the assumption of chemical equilibrium used in Fig. 2 and treat the quark and antiquark plasma as a freely flowing, decoupled system. The $q\bar{q}$ contribution to the decay of the background field can however not be neglected.

Color conductivity $\sigma_c(T)$ in this model is connected to the energy densities through the temperature. To be consistent with the assumption of decoupled, free-flowing quarks and antiquarks, we neglect the contribution from quarks and antiquarks to the color conductivity. This is well justified since even in total chemical equilibrium the relative increase in conductivity [Eq. (2)] is at most about 20% (because the plasma frequency increases while the mean free path decreases with inclusion of quarks).

For the evolution of the gluon plasma we include both the color conductivity and shear viscosity. The gluon temperature, energy density, and pressure are related in the Stefan-Boltzmann limit by $P_g = \epsilon_g/3$ and $T = (\epsilon_g/a_g)^{1/4}$, where $a_g = \pi^2\gamma_g/30$ with $\gamma_g = 16$.

The conductivity as defined by Eq. (2) is actually only an asymptotic value and is valid only for times greater than the momentum relaxation time. As discussed in Refs. [32–34, 19], when damping due to collisions are neglected plasma oscillations may arise in the system. Of course oscillations occur only if the product of the momentum degradation time τ_g and the plasma oscillation frequency ω_{pl} is large compared to π. Perturbatively, in the leading log approximation, $\tau_g\omega_{pl} \sim 0.4/\alpha_s^{3/2}\ln(1/\alpha_s) \sim \pi$ from Eq. (2). Therefore plasma oscillations are not likely to be important in a minijet plasma given the two-body damping rate. (Oscillations in the plasma at SPS energies may occur given the much smaller density of partons if the perturbative plasma picture can be extended down to such densities.)

In the overdamped approximation, a physical picture of the effective time dependence of the conductivity can be obtained by considering the equation of motion for a particle with a color charge g in an external field E_0:

$$\frac{dp_z}{d\tau} = -\frac{p_z}{\tau_g} + gE_0 \ . \tag{28}$$

With $p_z(0) = 0$ and neglecting the effect of the induced current on the external field, the solution is simply

$$p_z(\tau) = gE_0\tau_g(1 - e^{-\tau/\tau_g}) \ . \tag{29}$$

For partons with an effective mass, $\langle m\rangle$, the induced current becomes

$$\begin{aligned} j_z(\tau) &= \frac{g^2 n}{\langle m\rangle}\tau_g(1 - e^{-\tau/\tau_g})E_0 \\ &\approx \omega_{pl}^2\tau_g(1 - e^{-\tau/\tau_g})E_0 = \sigma_c^g(\tau)E_0 \ . \end{aligned} \tag{30}$$

In this limit the effective conductivity turns on as

$$\sigma_c^g(\tau) \approx (1 - e^{-\tau/\tau_g})\frac{T(\tau)}{\alpha_s\ln(1/\alpha_s)}, \tag{31}$$

where τ_g is given by Eq. (3).

At sufficiently early times the viscosity term in Eq. (6) is divergent. Physically, however, the viscosity in the kinetic limit can at most reduce the PdV work to zero. Therefore, we impose the condition that $P = 4\eta/(3\tau) = 0$ if $P \leq 4\eta/(3\tau)$. In this way free flow (without pressure) at early times turns into viscous flow at later times. However, the perturbative mean free paths for gluons turn out to be relatively long leading to a high shear viscosity. The evolution turns out to be close to near zero-pressure expansion at least at RHIC energies.

The final evolution equations are therefore

$$\begin{aligned} \frac{d\epsilon_g}{d\tau} + \frac{\epsilon_g}{\tau} = &-\left\{\frac{P_g(\tau)}{\tau} - \frac{4}{3}\frac{\eta_g(\tau)}{\tau^2}\right\}\Theta\left(P_g \geq \frac{4\eta_g}{3\tau}\right) \\ &+2\epsilon_f\left\{\kappa_g(2\epsilon_f)^{1/4} + \sigma_c^g(\tau)\right\} \\ &+\epsilon_h^g\frac{\tau_h}{\tau}\frac{\Theta(\tau_h \leq \tau \leq \tau_h + \delta)}{\delta}, \end{aligned} \tag{32}$$

$$\frac{d\epsilon_q}{d\tau}+\frac{\epsilon_q}{\tau}=\kappa(2\epsilon_f)^{5/4}+\epsilon_{\rm h}^q\frac{\tau_{\rm h}}{\tau}\frac{\Theta(\tau_{\rm h}\le\tau\le\tau_{\rm h}+\delta)}{\delta}, \quad (33)$$

$$\frac{d\epsilon_f}{d\tau}=-2\epsilon_f\left\{\kappa(2\epsilon_f)^{1/4}+\sigma_{\rm c}^g(T_g)\right\} +\epsilon_{\rm s}\frac{1}{\tau_f}\Theta(\tau_{\rm h}\le\tau\le\tau_f), \quad (34)$$

where $\kappa=\kappa_g+\kappa_q$ as given by Eq. (18) in the Abelian approximation. The perturbative result in the leading logarithm approximation for conductivity is given by (31) and for viscosity by (4). The resulting set of coupled equations is strongly nonlinear due to the sources and also conductivity and viscosity. Therefore these equations must be solved numerically.

We consider a central Au+Au collision at $\sqrt{s}=200A$ GeV with soft time scales fixed as $\tau_{\rm s}=1$ fm and $\tau_f=0.5$ fm. The hydrodynamic gluon plasma is decoupled at $\epsilon_g=\epsilon_{\rm c}=2$ GeV/fm^3 as in Fig. 2. The soft energy density scale $\epsilon_{\rm s}$ is determined as before. However, this has to be determined iteratively starting with an initial guess for $\epsilon_{\rm s}$ and evolving the equations to compute the final transverse energy E_T^0. We then modify the initial guess until E_T^0 converges to the HIJING prediction at $\sqrt{s}=20A$ GeV. The value thereby obtained for the field energy density is $\epsilon_{\rm s}\approx 4.9$ GeV/fm^3.

The time evolution of energy densities and the transverse energy at central rapidity are shown in Figs. 3 as functions of the proper time τ. Figure 3(a) represents the evolution of the total energy density $\epsilon(\tau)=\epsilon_g(\tau)+\epsilon_q(\tau)$. Curve "1" is the result an ideal (free) Bjorken expansion (no conductivity, no pressure, no viscosity). Curve "4" is the minijet contribution in the Bjorken flow. Curve "2" is the solution with the perturbative estimates for the conductivity and viscosity. Onset of conductivity is taken into account according to (31). Since the leading log approximation is good only within a factor of 2, we have studied also the consequences of having $\tau_g=\tau_g^{\rm pQCD}/2$, which is shown by curve "3." Evolution of the total transverse energy at the central rapidity is plotted in Fig. 3(b) for the respective cases. The decomposition of the total energy density is then shown in Fig. 3(c), and the evolution of the field energy density is displayed in Fig. 3(d). Also in the two latter figures we again show both the case $\tau_g=\tau_g^{\rm pQCD}$ and $\tau_g=\tau_g^{\rm pQCD}/2$.

We note the following points in Fig. 3.

1. The spread of the minijet production times due

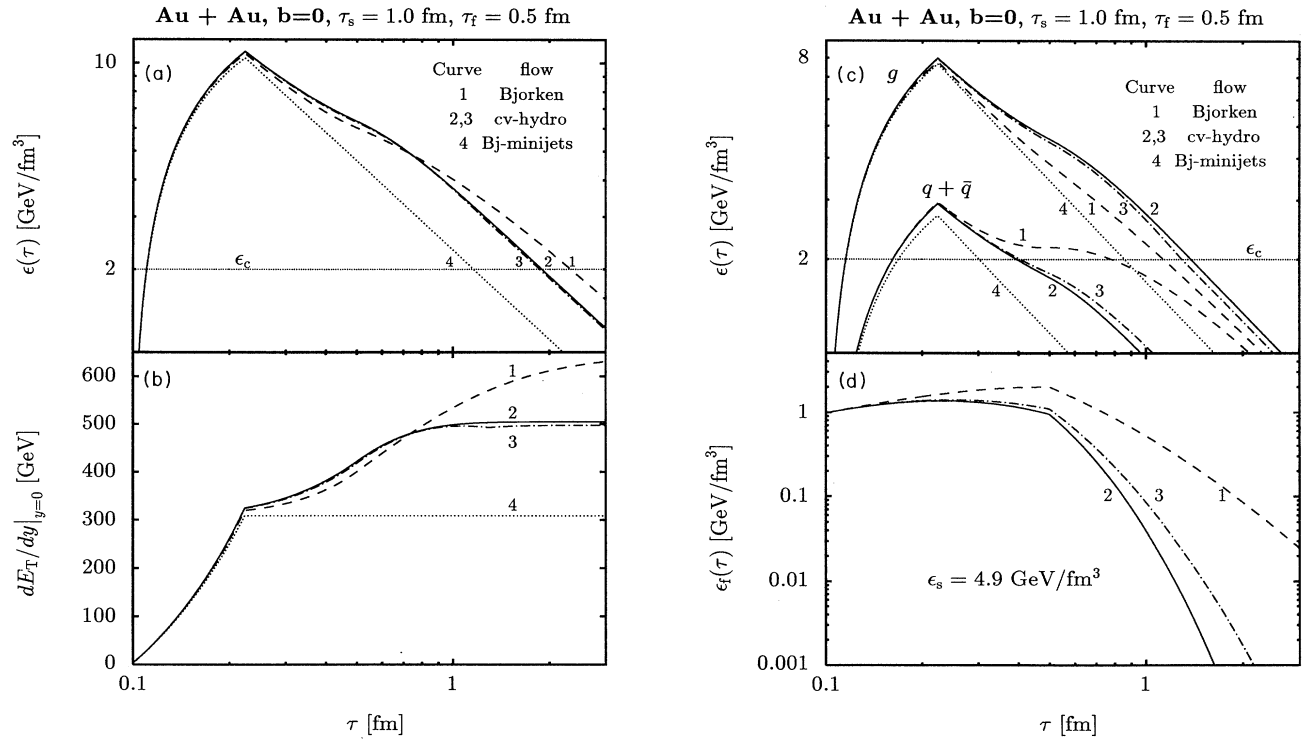

FIG. 3. Evolution of the minijet plasma with minijet initial conditions and decoupled fermions given by Eqs. (32)–(34). Curves 1 correspond to nonconductive, nonviscous free flow. Curves 4 show the pure minijet contribution to curve 1. Curves 2 show the solution of the equations with the perturbative estimates for the viscosity and conductivity. Curves 3 show the solution when the momentum relaxation time τ_g is reduced by a factor of 2. For curves 2 and 3 the gluon component is assumed to decouple at $\epsilon_{\rm c}=2$ GeV/fm^3. In parts a and b, the evolution of the total energy density and the total transverse energy are shown to compare with Fig. 2. In part c, the decomposition of the energy density into gluonic and quark components is shown. In part d, the evolution of the field energy density in nonconductive (1) and conductive (2 and 3) cases is shown. See text for discussion of results.

to the finite nuclear thickness lowers the maximum energy densities by about a factor of 2 relative to Fig. 2(a) at RHIC energies. (The kinks in the curves result from the assumed sharp edge nuclear geometry which are smoothed out with diffuse nuclei.)

2. Figure 3(d) shows clearly how the minijet enhanced conductivity (curves 2 and and 3) quenches the background field much faster than in the nonconductive case (curve 1). With a shorter mean free path, the asymptotic value of conductivity is decreased, but the early time dependence of it is only weakly dependent on the relaxation time. This is why the difference between curves 2 and 3 is so small. Notice also how a finite formation time of the field causes the field energy density to remain approximately constant at a much smaller value ~ 1 GeV/fm^3 than in Fig. 2.

3. In Fig. 3(c) note that in the nonconductive Bjorken flow (curve 1) the $q\bar{q}$ energy density at $\tau > \tau_f = 0.5$ fm remains above ϵ_c for a relative long time due pair production from the background field. The gluonic energy density is much less affected because of the dominant minijet contribution.

4. In the conductive flow [curves 2 and 3 in Fig. 3(c)] much fewer $q\bar{q}$ pairs are produced by the quenched background field for $\tau > \tau_f$.

5. The effects of Ohmic heating is clearly seen in Fig. 3(c) comparing curves 2 and 3 to 1. Unlike the $q\bar{q}$ energy density, the gluon energy density exceeds the Bjorken curve due to the conversion of field energy into heat.

6. With the perturbative estimate leading to a large shear viscosity, we note that at RHIC energies the effect of PdV work is mostly neutralized compared to curve 3 in Fig. 2. Even reducing the perturbative momentum degradation time by a factor of 2 [curve 3 in Fig. 3(c)] does not lead to a dramatic effect. At higher cms energies, however, we expect hydrodynamic flow to have stronger influence on the evolution of the system (cf. Fig. 2).

7. Note in Fig. 3(c) that curves 2 and 3 are reversed for $q\bar{q}$ relative to gluons because a reduced conductivity increases the time available for $q\bar{q}$ pair production. In Fig. 3(a) the total energy density is therefore remarkably insensitive to the numerical value of the conductivity. The same is true for the transverse energy evolution in Fig. 3(b).

8. Curves 2 and 3 in Figs. 3(a) and 3(b) reveal the small net effect of conductive viscous flow. At early times ~ 0.2–0.5 fm, Ohmic heating maintains a slightly higher value of the energy density relative to the free streaming case. However, at later times viscous expansion cools the system somewhat below the free streaming curve 1.

9. The final dE_T/dy in conductive viscous flow is reduced by approximately 150 GeV compared to the free streaming (HIJING) case (curve 1). In comparison the ideal hydrodynamic evolution in Fig. 2 is seen to reduce the transverse energy per unit rapidity by approximately 250 GeV.

10. The above results are found to be very insensitive to the parameters of the model. We found that changing τ_s from 1 fm to 0.5 fm, which changes ϵ_s from 4.9 GeV/fm^3 to 8.1 GeV/fm^3 and α_s from 0.42 to 0.67, changes the final transverse energy at midrapidity only by about 5%.

VI. CONCLUSIONS

In this paper we studied possible consequences of color conductivity on the evolution of the minijet gluon plasma produced in Au+Au at RHIC energies. We also included effects of shear viscosity in the Navier-Stokes approximation. We started with minijet initial conditions at RHIC energies, as determined by first-order perturbative QCD, and evolved the plasma according to the chromoviscous-hydrodynamic equations with approximate longitudinal boost invariant initial conditions. In the context of the flux tube model for beam jet fragmentation, we showed that the gluonic conductivity damps rapidly the background color field. Ohmic heating keeps the energy density above the critical point slightly longer than in the case of free streaming but work done on viscous expansion reduces the final transverse energy by $\sim 25\%$.

The strongest effect of conductive flow in our calculation is the suppression of $q\bar{q}$ production from the background field shown in Fig. 3(c). We have emphasized that most of the minijets are gluons and the system is initially far from being in a chemical equilibrium with respect to quarks and gluons. The primary effect of color conductivity seems to be to hinder chemical equilibration by reducing the source of $q\bar{q}$ pairs. Without conductivity the background color field produces sufficiently many $q\bar{q}$ pairs that near ϵ_c chemical equilibrium may be more nearly achieved. However, with the enhanced minijet conductivity the ratio of q to g densities remain far below equilibrium at least above the critical temperature. This calculation provides therefore an explicit dynamical realization of the van Hove–Pokorski [35] picture of high-energy reactions as dominated by gluonic interactions.

We close by emphasizing several caveats and open problems. We considered the background field decay in the Abelian approximation to overestimate deliberately the $q\bar{q}$ production rate. As discussed in [17, 27], in the SU(3) case the field decays practically equally to fermions and bosons. This should have the effect of suppressing further the $q\bar{q}$ component. Also we have not included initial nor final state branching of minijets that predominantly enhances the gluon number density. At LHC energies the approximation of decoupling the quark plasma must be relaxed because of the longer time scale for the plasma to remain above ϵ_c.

At RHIC energies the hindrance of soft $q\bar{q}$ production may reduce the dilepton production rate expected from equilibrium estimates. Most studies [36–39] have assumed implicitly chemical equilibration in computing $q\bar{q}$ annihilation from the quark-gluon plasma. In Ref. [39], for example, it was suggested that the rates for thermal dilepton production are well above the Drell-Yan rates near $M \sim 3$ GeV at collider energies. However, rapid chemical equilibration and high initial temperatures were essential for that conclusion. We have seen that the minijet gluon plasma has difficulty achieving chemical equilibration during the pure plasma phase $\tau < 2$ fm at least at RHIC energies. The reduced density of quarks and antiquarks may therefore reduce significantly the number of hard photons and dilepton pairs relative to those equilibrium estimates. On the other hand, the reduc-

tion of the dilepton yield due to chemical nonequilibrium could be compensated for by other nonequilibrium effects. In particular, a strong deviation from local momentum space equilibrium, e.g., with $\langle p_z^2 \rangle \gg \langle p_T^2 \rangle/2$ due to the the induced color current or the initial-state momentum anisotropy, may enhance the yields significantly beyond equilibrium estimates [33, 40, 41]. Much more work remains to reduce the uncertainties caused by these competing effects.

Finally, we showed that chromoviscous expansion of the minijet plasma may lead to a modest reduction $\sim 25\%$ of the transverse energy production relative to free streaming (e.g., HIJING [5]) dynamics. The free streaming value estimated for central AuAu collisions is, however, uncertain by $\sim 50\%$ because of the unknown scaling of the minijet scale $p_0(A, s)$, nuclear shadowing, and beam jet fragmentation. Therefore, transverse energy measurements must be supplemented by detailed systematic measurements of a wide variety of other observables as discussed in [9].

ACKNOWLEDGMENTS

We acknowledge helpful discussions with X.-N. Wang, T. Matsui, and K. Kajantie. K.J.E. is grateful to the Academy of Finland, Emil Aaltonen Foundation, and Magnus Ehrnrooth Foundation for partial financial support. This work was supported by the Office of Energy Research, Division of Nuclear Physics of the Office of High Energy and Nuclear Physics of the U.S. Department of Energy under Contract Nos. DE-AC03-76SF00098, DE-FG05-90ER40592, and DE-FG02-93ER40764.

[1] K. Kajantie, P. V. Landshoff, and J. Lindfors, Phys. Rev. Lett. **59**, 2527 (1987).
[2] J.P. Blaizot and A.H. Mueller, Nucl. Phys. **B289**, 847 (1987).
[3] K. J. Eskola, K. Kajantie, and J. Lindfors, Nucl. Phys. **B323**, 37 (1989).
[4] G. Calucci and D. Treleani, Phys. Rev. D **41**, 3367 (1990); **44**, 2746 (1991).
[5] X.-N. Wang and M. Gyulassy, Phys. Rev. D **44**, 3501 (1991).
[6] X.-N. Wang and M. Gyulassy, Phys. Rev. D **45**, 844 (1992).
[7] X.-N. Wang and M. Gyulassy, Phys. Rev. Lett. **68**, 1480 (1992).
[8] M. Gyulassy, M. Plümer, M. Thoma, and X.-N. Wang, in *Intersections Between Particle and Nuclear Physics*, Proceedings of the Fourth Conference on the Intersections between Particle and Nuclear Physics, Tucson, AZ, 1991, edited by W. T. H. van Oers (AIP, New York, 1991).
[9] *Quark Matter '91*, Proceedings of the Ninth International Conference on Ultra-Relativistic Nucleus-Nucleus Collisions, Gatlinburg, TN, 1991, edited by T. C. Awes *et al.* [Nucl. Phys. **A544**, 1c (1992)].
[10] U. Heinz, Ann. Phys. (N.Y.) **168**, 148 (1986).
[11] S. Mrówczyński, Acta Phys. Pol. **B19**, 91 (1988).
[12] S. Mrówczynski, in *Quark-Gluon Plasma*, edited by R. Hwa (World Scientific, Singapore, 1990).
[13] G. Gatoff, A. K. Kerman, and T. Matsui, Phys. Rev. D **36**, 114 (1987).
[14] P. Danielewicz and M. Gyulassy, Phys. Rev. D **31**, 53 (1985).
[15] A. Casher, H. Neuberger, and S. Nussinov, Phys. Rev. D **20**, 179 (1979).
[16] N. K. Glendenning and T. Matsui, Nucl. Phys. **B245**, 449 (1984).
[17] M. Gyulassy and A. Iwazaki, Phys. Lett. **165B**, 157 (1985).
[18] K. Kajantie and T. Matsui, Phys. Lett. **164B**, 373 (1985).
[19] Y. Kluger, J. M. Eisenberg, B. Svetitsky, F. Cooper, and E. Mottola, Phys. Rev. D **45**, 4659 (1992); Phys. Rev. Lett. **67**, 2427 (1991); Report No. TAUP 2006-92, 1992 (unpublished).
[20] G. Gatoff, A. K. Kerman, and D. Vautherin, Phys. Rev. D **38**, 96 (1988).
[21] B. Andersson *et al.*, Phys. Rep. **97**, 31 (1983); Nucl. Phys. **B281**, 289 (1987).
[22] G. Marchesini and B. R. Webber, Nucl. Phys. **B310**, 461 (1988).
[23] G. Baym, H. Monien, C. J. Pethick, and D. G. Revenhall, Phys. Rev. Lett. **64**, 1867 (1990).
[24] S. Gavin, Nucl. Phys. **A435**, 826 (1985).
[25] A. Hosoya and K. Kajantie, Nucl. Phys. **B250**, 666 (1985).
[26] J. D. Bjorken, Phys. Rev. D **27**, 140 (1983).
[27] M. Gyulassy, H.-Th. Else, A. Iwazaki, and D. Vasak, *Pair Production and Quantum Transport in Strong Color Fields*, in *Physics of Strong Fields*, Proceedings of a NATO Advanced Study Institute on Physics of Strong Fields, Maratea, Italy, 1986, edited by W. Greiner (Plenum, New York, 1987).
[28] X.-N. Wang, Phys. Rev. D **43**, 104 (1991).
[29] N. Abou-El-Naga, K. Geiger, and B. Müller, J. Phys. G **18**, 797 (1992).
[30] K. J. Eskola, Nucl. Phys. B (to be published).
[31] D. W. Duke and J. F. Owens, Phys. Rev. D **30**, 49 (1984).
[32] A. Bialas and W. Czyż, Acta Phys. Pol. **B17**, 635 (1986).
[33] M. Asakawa and T. Matsui, Phys. Rev. D **43**, 2871 (1991).
[34] F. Cooper, *Dynamical Approach to Pair Production from Strong Color Fields*, Lectures given at a NATO Advanced Study Institute on Particle Production in Highly Excited Matter, Il Ciocco, Italy, 1992 (Report No. LA-UR-92-2753).
[35] L. van Hove and S. Pokorski, Nucl. Phys. **B86**, 243 (1975).
[36] K. Kajantie and P. V. Ruuskanen, Z. Phys. C **44**, 167 (1989).
[37] P. V. Ruuskanen, in *Proceedings of the International Workshop on Quark Gluon Plasma Sigantures*, Strasbourg, France, 1990, edited by A. Capella *et al.* (Editions Frontieres, Gif-sur-Yvette Cedex, 1991).
[38] P. V. Ruuskanen, in [9], p. 169c.
[39] J. I. Kapusta, L. McLerran, and D. K. Srivastava, Phys. Lett. B **283**, 145 (1992).
[40] B. Kämpfer and O. P. Pavlenko, Phys. Lett. B **289**, 127 (1992).
[41] K. Geiger and J. I. Kapusta, Phys. Rev. Lett. **70**, 1290 (1993).